JOURNAL OF SOLID STATE CHEMISTRY 105, 363–370 (1993)

A New "123" Family: $LnBa_2Fe_3O_z$. (II). Ln = Nd, Sm, and Eu

E. GARCÍA-GONZÁLEZ,*,† M. PARRAS,*
J. M. GONZÁLEZ-CALBET,*,‡,§ AND M. VALLET-REGÍ‡,¶

Departamento de Química Inorgánica, Facultad de Químicas, Universidad Complutense, 28040-Madrid, Spain; ‡Instituto de Magnetismo Aplicado, RENFE-UCM, Apdo. Correos 155, 28230-Las Rozas (Madrid), Spain; and ¶Departamento de Química Inorgánica y Bioinorgánica, Facultad de Farmacia, Universidad Complutense, 28040-Madrid, Spain

Received August 4, 1992; in revised form November 23, 1992; accepted November 23, 1992

The microstructural characterization of $Nd_{1/3}Ba_{2/3}FeO_{2.80}$ material has been studied by means of electron diffraction and high resolution electron microscopy. A structural model in which two square pyramids alternate with three octahedra along the [001] direction is proposed. The material can be described as the $n = 2$ term of the $Ln_{1/3}Ba_{2/3}FeO_{3-(1/2n+1)}$ family. The same study developed on $Sm_{1/3}Ba_{2/3}FeO_{2.78}$ and $Eu_{1/3}Ba_{2/3}FeO_{2.76}$ reveals a more complex microstructure, exhibiting a short-range order situation.

Introduction

In order to create anionic deficiency in the ABO_3 perovskite structure, it is possible to modify the composition in the A (cationic) sublattice. Much work has been devoted to the $AA'FeO_{3-y}$ materials (*1–3*) and the anionic vacancies distribution being governed, among others, by two main factors: the relative stability of the different iron sites and the $A:A'$ ratio. Gibb and Matsuo (*4*) have studied the $Ba_xLa_{1-x}FeO_{3-y}$ system by means of Mössbauer spectroscopy, observing a continuous decrease of the iron on tetrahedral sites when the Ba content is increased; for $x = 0.5$, the tetrahedral sites almost disappear at the expense of the fivefold site appearance.

In the $LaFeO_3$–$Ca_2Fe_2O_5$ perovskite-related system, compositional variations lead to the $LaCa_2Fe_3O_8$ ordered phase (1 : 2 : 3), where two octahedral layers alternate with a tetrahedral layer along the c-axis, the stacking sequence being . . . OOTOOT . . . (O, octahedron, T, tetrahedron) (*1*).

When Ca is substituted by Ba in the above 1 : 2 : 3 phase, two different situations can occur depending on the Fe(IV) content, i.e., on the oxygen content. When it contains 38% of Fe(IV) ($Ba_{2/3}La_{1/3}FeO_{2.85}$) a simple cubic phase is obtained (*5*); however, when all iron is found in the III oxidation state ($Ba_{2/3}La_{1/3}FeO_{2.67}$), the material appears to be formed by three-dimensional microdomains (*6*): the unit cell corresponding to each domain is related to the cubic perovskite structure by the expression $a_c \times a_c \times 2a_c$ (a_c being the cubic perovskite unit cell parameter).

In a previous paper (*7*), we reported that $Dy(Ho)Ba_2Fe_3O_8$ materials can also be described as a threefold perovskite superstructure, the stacking sequence being . . . POPPOP . . . (P, square pyramid). The substitution of dysprosium or holmium by neodymium, samarium, or europium leads to a different anionic vacancy rearrangement. Microstructural characteriza-

† Work submitted in part for the fulfillment of the degree of Doctor of Chemistry by E.G.G., Universidad Complutense, Madrid, April 1992.

§ To whom correspondence should be addressed.

0022-4596/93 $5.00

TABLE I

ANIONIC COMPOSITION OF THE $Ln_{1/3}Ba_{2/3}Fe_{3-y}$ MATERIALS

Ln	% Fe(IV)	Composition
Nd	27	$Nd_{1/3}Ba_{2/3}FeO_{2.80}$
Sm	21	$Sm_{1/3}Ba_{2/3}FeO_{2.78}$
Eu	20	$Eu_{1/3}Ba_{2/3}FeO_{2.76}$
Dy	—	$Dy_{1/3}Ba_{2/3}FeO_{2.67}$
Ho	—	$Ho_{1/3}Ba_{2/3}FeO_{2.67}$

tion by means of selected area electron diffraction (SAED) and high resolution electron microscopy (HREM) has been carried out to solve these differences.

Experimental

Samples of nominal composition $Ba_{2/3}Ln_{1/3}FeO_{3-y}$ (Ln = Nd, Sm, and Eu) were prepared by heating stoichiometric mixtures of $BaCO_3$, Ln_2O_3, and α-Fe_2O_3 of annalaR quality at 1300°C for 72 hr in air. The homogeneous black products were quenched to room temperature in the platinum crucibles used for synthesis.

The oxidation state of iron was determined by titration after dilution in 3 *N* HCl with an excess of Mohr salt.

Powder X-ray diffraction was performed on a Siemens D-5000 diffractometer with a graphite monochromator and using Cu$K\alpha$ radiation.

Electron diffraction was carried out on a JEOL 2000FX electron microscope, fitted with a double tilting goniometer stage (±45°). High resolution electron microscopy was performed on a JEOL 4000EX electron microscope, fitted with a double tilting goniometer stage (±25°) by working at 400 kV. The samples were ultrasonically dispersed in *n*-butanol and transferred to carbon-coated copper grids.

Results and Discussion

The average composition of the samples, as deduced by chemical analysis, is shown in Table I. It can be seen that the Fe(IV) amount decreases when the lanthanide element becomes smaller. In fact, when the lanthanide element is dysprosium or holmium, all iron is found in the (III) oxidation state (*7*).

Although X-ray diffraction patterns can be indexed on the basis of a pseudocubic perovskite phase, the microstructural studies developed by means of electron microscopy show a more complex situation. Figures 1A, 1B, and 1C show the SAED patterns along the $[001]_c$, $[0\bar{1}1]_c$, and $V[\bar{1}11]_c\|$ zone axes, respectively, for $Nd_{1/3}Ba_{2/3}FeO_{2.80}$. All maxima can be indexed as corresponding to the simple cubic perovskite. However, the SAED patterns along the $[010]_c$ and $[1\bar{1}0]_c$ zone axes (Figs. 2A and 2B), show a fivefold superstructure along the c^* cubic axis. This is reflected on the corresponding high resolution images (Figs. 3A and 3B), which reveal the presence of lattice fringes at 1.95 nm ($\approx 5a_c$) along the $[001]_c$ direction in a well ordered material.

The above results lead to a reciprocal lattice corresponding to a tetragonal symmetry real space cell of parameters $a_c \times a_c \times 5a_c$, and *P4/mmm* as a possible space group.

The cation occupying the *A* positions in the perovskite cell highly influences the relative stability of the different iron environments. The stability of tetrahedral and octahedral coordination of iron in the $Ca_{1-x}La_xFeO_y$ and $Sr_{1-x}La_xFeO_y$ systems has been established (*8–10*). However, when Ca or Sr are replaced by Ba, iron can also adopt fivefold coordination (*4, 11, 12*).

According to the oxygen composition determined by chemical analysis and taking into account the ability of iron to adopt tetrahedral, square-pyramidal, and octahedral coordinations, the two following vacancy distributions would lead to a fivefold superstructure:

—a sequence constituted by four octahedra and one tetrahedron along the $[001]_c$ direction,

‖ Subindex c refers to the basic perovskite cubic subcell.

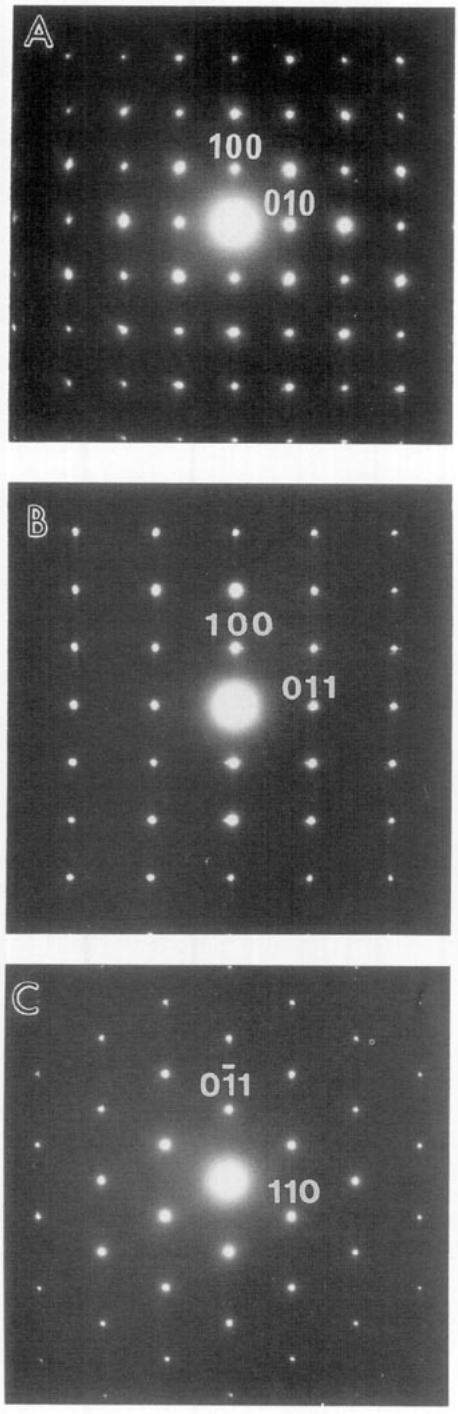

FIG. 1. Electron diffraction patterns corresponding to the $Nd_{1/3}Ba_{2/3}FeO_{2.80}$ material along the (A) $[001]_c$, (B) $[0\bar{1}1]_c$, and (C) $[\bar{1}11]_c$ zone axes.

—a stacking sequence formed by three octahedra and two square pyramids along the $[001]_c$ direction.

The first possibility would give the hypothetical $n = 5$ term of the homologous series $A_nB_nO_{3n-1}$ (*1*). The ordering of the anionic vacancies along $[110]_c$ giving rise to tetrahedral sites, and the relative orientation of the tetrahedra along the c axis would lead to an orthorhombic unit cell of parameters $\simeq a_c\sqrt{2} \times a_c\sqrt{2} \times 10a_c$ (space group *Pnma* (*13*)). However, the lack of systematic absences and diffraction maxima doubling both the $[110]_c$ and $[1\bar{1}0]_c$ directions, allow us to reject this model.

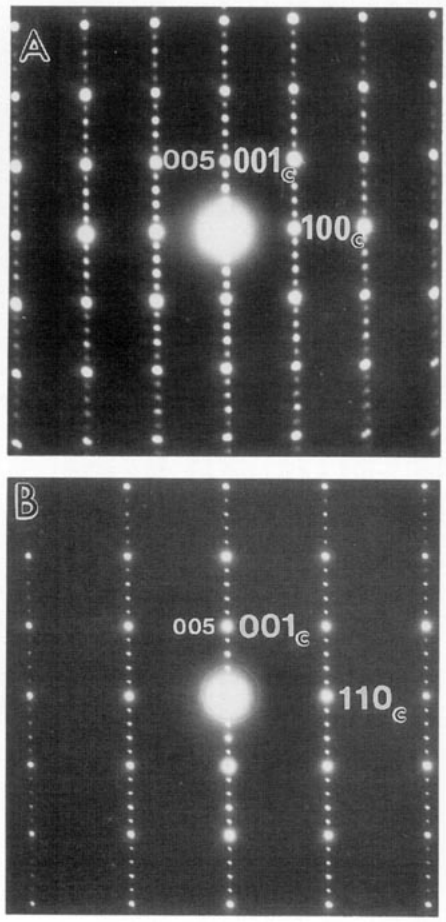

FIG. 2. Electron diffraction patterns for $Nd_{1/3}Ba_{2/3}FeO_{2.80}$ along the (A) $[010]_c$ and (B) $[1\bar{1}0]_c$ zone axes.

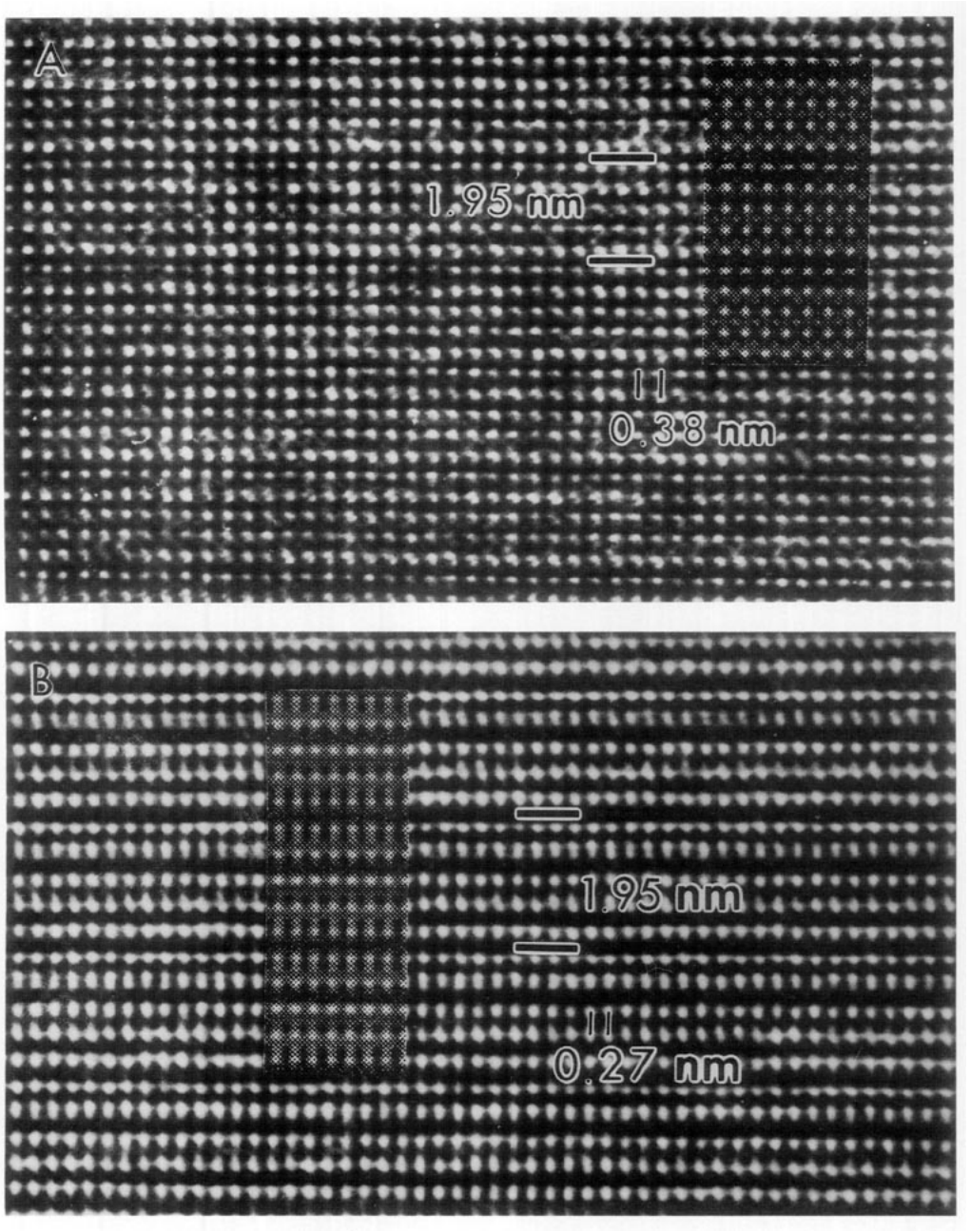

FIG. 3. High resolution images for the $Nd_{1/3}Ba_{2/3}FeO_{2.80}$ material and corresponding calculated images along the (A) $[010]_c$ and (B) $[1\bar{1}0]_c$ zone axes.

The relative order of the $[FeO_5]$ and $[FeO_6]$ polyhedra can give rise to two different stacking sequences along the $[001]_c$ direction, . . . |PPOOO|PPOOO| . . . and . . . |OPOPO|OPOPO| . . . . The interpretation of the image contrast in the high resolution images obtained has also been made with the help of a simulation program using the multislice method (*14*). The image calculation leads to the best fitting for the second sequence.

The ensemble of these results allows us

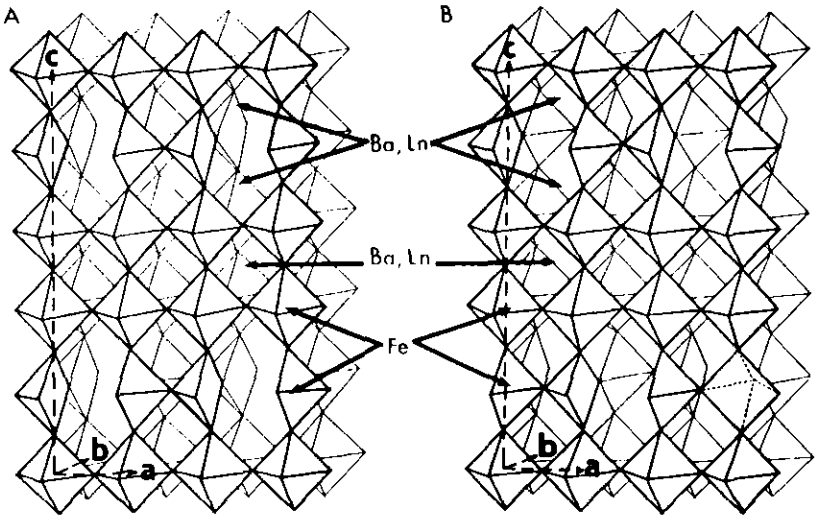

FIG. 4. Structural model for $Nd_{1/3}Ba_{2/3}FeO_{2.80}$: (A) ordered vacancy distribution and (B) random vacancy distribution.

to propose the structure model represented in Fig. 4A. It is constituted by the alternation of $[FeO_5]$ and $[FeO_6]$ polyhedra in such a way that the oxygen vacancies are ordered along the $[010]_c$ and $[100]_c$ direction in one of each two (005) planes. However, such a distribution would imply order in the relative orientation of the square pyramidal sites and thus, the doubling of either the [010] or [100] direction.

Attempts to interpret the structure based on complete ordering of O vacancies have been unsuccessful, with discrepancies between the observed and calculated intensities of particular superstructure reflexions, indicating, to some extent, that the O vacancy distribution is statistical. The absence of diffraction spots at $(\frac{1}{2}\ 0\ 0)$ or $(0\ \frac{1}{2}\ 0)$ suggests that, probably, the oxygen vacancies are disordered in the **ab** plane. Thus, the vacancy distribution in the five FeO_2 layers along the **c** axis is statistical but an oxygen defective layer always alternates with one filled layer in the **c** direction. According to that, the proposed structural model is represented in Fig. 4B. The superstructure reflexions can then be attributed, first, to an ordered distribution of O vacancies along the **c** axis and, secondly, to a displacement of oxygens and metal atoms from their positions in the fundamental perovskite-type structure.

Image calculations were carried out under the following imaging conditions: sample thickness between 1.7 and 5.5 nm; $\Delta f = -30$ to -70 nm; Cs = 1.0 nm; Cc = 1.7 nm; beam divergence angle = $0.8\ 10^{-3}$ rad; and accelerating voltage = 400 kV.

The structure model used for simulating images is the one represented on Fig. 4B, along the $[010]_c$ and $[1\bar{1}0]_c$ projections. The agreement is satisfactory for the following conditions:

—$[010]_c$ projection: $\Delta f = -60$ nm and sample thickness of 4.0 nm.

—$[1\bar{1}0]_c$ projection: $\Delta f = -60$ nm and sample thickness of 3.0 nm.

Both images are inset on Figs. 3A and 3B, respectively.

For the $Sm_{1/3}Ba_{2/3}FeO_{2.78}$ and $Eu_{1/3}Ba_{2/3}FeO_{2.76}$ materials (see Table I), only a small percentage of crystals presented the fivefold superstructure, the others showing a short range order situation probably due to the lower oxygen content of these materials. Effectively, Figs. 5A and 5B show the high

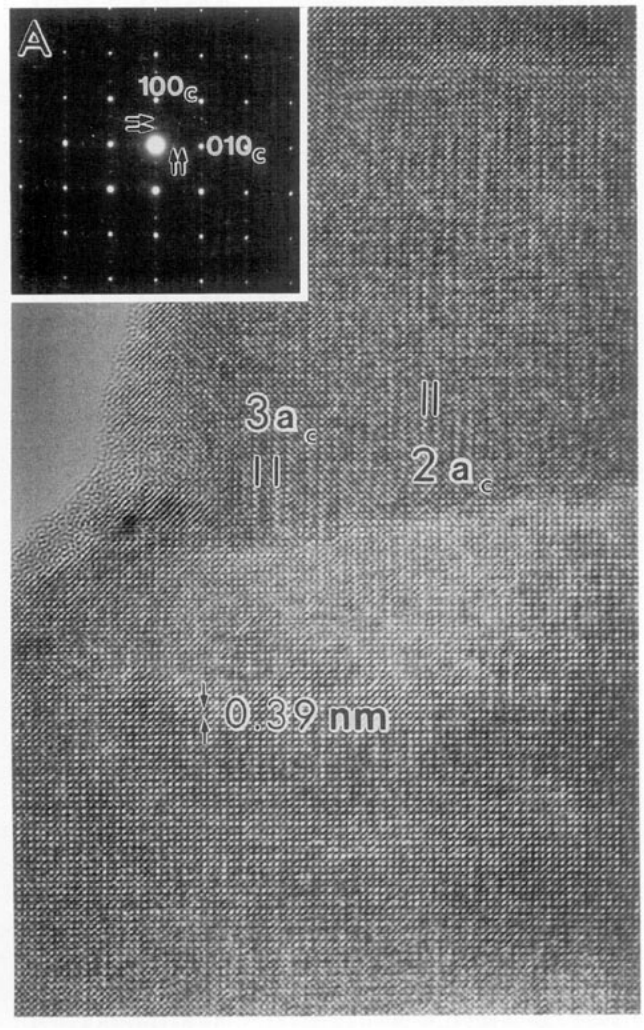

FIG. 5. High resolution images for $Sm(Eu)_{1/3}Ba_{2/3}FeO_{3-y}$ along the (A) $[001]_c$ and (B) $[1\bar{1}0]_c$ zone axes. The corresponding electron diffraction patterns are shown as insets: arrows indicate the position of satellite reflections.

resolution images along the $[001]_c$ and $[1\bar{1}0]_c$ zone axes, respectively, for $Sm_{1/3}Ba_{2/3}FeO_{2.78}$. The corresponding SAED patterns are inset on each image.

The electron diffraction pattern along the $[001]_c$ zone axis (inset on Fig. 5A), is dominated by a set of strong matrix reflections $\mathbf{G}_{hkl}$ corresponding to the perovskite substructure and a weaker set of inconmensurate satellite reflections at $\mathbf{G} \pm m\mathbf{q}$, m being an integer and $\mathbf{q} \simeq \frac{2}{5}\mathbf{a}^*$. These satellite reflections appear also along the $\mathbf{b}^*$ direction. Besides, the corresponding image reveals the crystals as being formed by three-dimensional microdomains. By tilting around $\mathbf{a}^*$ (see inset on Fig. 5B) the electron diffraction pattern along the $[1\bar{1}0]$ zone axis shows the same satellite reflections along $\mathbf{a}^*$, with the same value of the modulation vector $\mathbf{q}$.

High resolution images of Figs. 5A and 5B show contrast variations along $\mathbf{a}$ that cor-

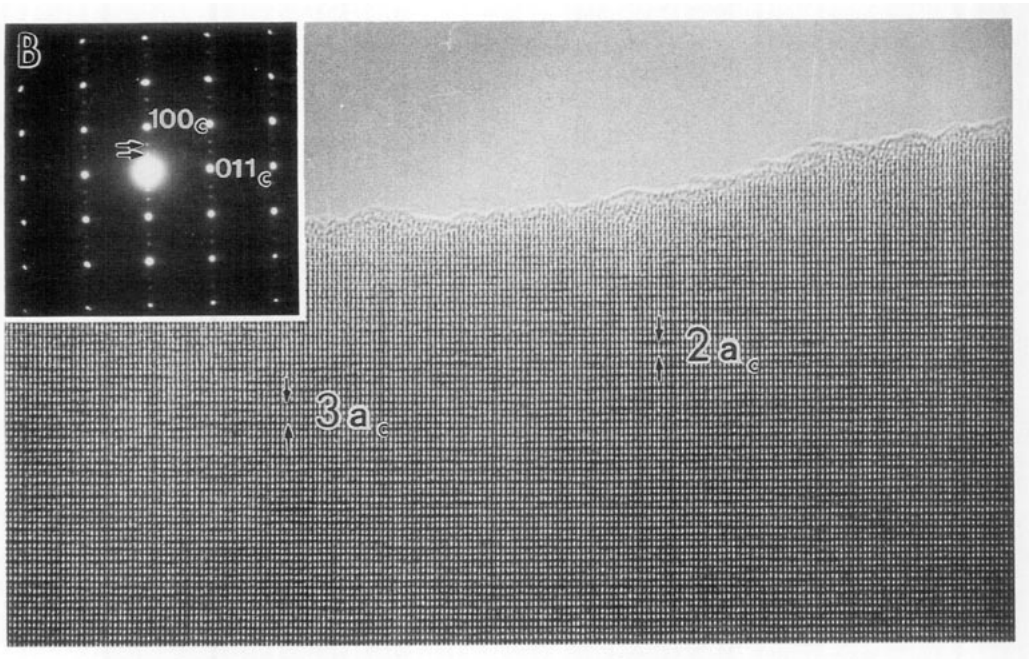

FIG. 5—*Continued*

respond to twice and triple the perovskite subcell parameter a_c. The 1 : 1 ratio of both types of spacing in the crystal would lead to the appearance of satellite reflections at exactly $\mathbf{q} = \frac{2}{5}\mathbf{a}^*$. Careful mesurements of the **q** value on several crystals indicate smooth variations from crystal to crystal (in the 0.39–0.40 range) probably due to the disordered distribution of both types of spacing along **a**.

When the anionic composition corresponds to $3 - y = 2.80$, and the two types of spacing are in a 1 : 1 ratio and distributed in an ordered way, the satellite reflections become superlattice (conmensurate) reflections (see Figs. 2 and 3), and it can be assumed that the modulation occurs as an "intermediate state" previous to this well ordered composition.

Taking into account the above results for the $Nd_{1/3}Ba_{2/3}FeO_{2.80}$ material, and according to the previously reported structural model proposed for the $Dy(Ho)_{1/3}Ba_{2/3}FeO_{2.67}$ material (*7*) (alternation of two square pyramids [FeO_5] and one octahedron [FeO_6] along the **c** axis), it can be assumed the formation of two different terms of the $Ln_{1/3}Ba_{2/3}FeO_{3-(1/2n+1)}$ family, where the $n = 1$ term is constituted by the $Dy(Ho)_{1/3}Ba_{2/3}FeO_{2.67}$ material and the $n = 2$ term is the $Nd_{1/3}Ba_{2/3}FeO_{2.80}$ phase. Higher n values would correspond to terms of composition closer to the ABO_3 stoichiometry, which would constitute the $n = \infty$ term.

It is worth mentioning that each anionic composition is associated with the lanthanide element considered at the above synthesis conditions. This fact does not exclude the possibility of preparing different anionic compositions for the same lanthanide element varying the experimental method and thus leading to other terms of this family. Although the A cations are disordered, the 1 : 2 ratio seems to be necessary. Different $A : A'$ ratios would lead to $LnFeO_3$-type orthorhombic phases (for low barium contents) or to biphasic compositions (for high barium contents) (*15*). Moreover, several investigations concerning to various $A : A'$ ratios in the La–Ba–Fe–O system seem to

indicate that the presence of barium is highly connected with the apperance of fivefold sites for iron (*4, 5*).

More studies to elucidate whether or not these hypotheses are true are in progress and will be reported in due course.

Acknowledgments

We acknowledge the financial support of C.I.C.Y.T. (Spain), through Research Projects MAT 90-0858-C02-02 and MAT 91-0331, and MIDAS Program. E.G.G. also thanks the Spanish Ministry of Education for a supporting grant. We are also grateful to Mr. A. García for valuable technical assistance.

References

1. J. C. GRENIER, M. POUCHARD, AND P. HAGENMULLER, *Struc. Bonding* **47,** 1 (1981).
2. J. M. GONZÁLEZ-CALBET, M. VALLET-REGÍ, M. ALARIO-FRANCO, AND J. C. GRENIER, *Mater. Res. Bull.* **18,** 285 (1983).
3. J. M. GONZÁLEZ-CALBET AND M. VALLET-REGÍ, *J. Solid State Chem.* **68,** 226 (1987).
4. J. C. GIBB AND M. MATSUO, *J. Solid State Chem.* **81,** 83 (1989).
5. M. PARRAS, M. VALLET-REGÍ, J. M. GONZÁLEZ-CALBET, AND J. C. GRENIER, *J. Solid State Chem.* **74,** 322 (1988).
6. J. M. GONZÁLEZ-CALBET, M. PARRAS, M. VALLET-REGÍ, AND J. C. GRENIER, *J. Solid State Chem.* **92,** 110 (1991).
7. E. GARCÍA-GONZÁLEZ, M. PARRAS, J. M. GONZÁLEZ-CALBET, AND M. VALLET-REGÍ, *J. Solid State Chem.* **104,** 232 (1993).
8. J. C. GRENIER, L. FOURNES, M. POUCHARD, P. HAGENMULLER, AND S. KOMORNICKI, *Mater. Res. Bull.* **17,** 55 (1982).
9. P. D. BATTLE, T. C. GIBBS, AND S. NIXON, *J. Solid State Chem.* **79,** 75 (1989).
10. P. D. BATTLE, T. C. GIBBS, AND S. NIXON, *J. Solid State Chem.* **79,** 86 (1989).
11. M. PARRAS, L. FOURNES, J. C. GRENIER, M. POUCHARD, M. VALLET, J. M. GONZÁLEZ-CALBET, AND P. HAGENMULLER, *J. Solid State Chem.* **88,** 261 (1990).
12. X. ZOU, S. HÖVMOLLER, M. PARRAS, J. M. GONZÁLEZ-CALBET, M. VALLET-REGÍ, AND J. C. GRENIER, *Acta Crystallogr. A* **49,** 27 (1993).
13. S. HOVMÖLLER, X. ZOU, D. W. WANG, J. M. GONZÁLEZ-CALBET, AND M. VALLET-REGÍ, *J. Solid State Chem.* **77,** 316 (1988).
14. NCEMSS Program, National Center for Electron Microscopy, Materials and Chemical Sciences Division, Lawrence Berkeley Laboratory. University of California, Berkeley, California, 1989.
15. Unpublished results.